Science of the Total Environment 920 (2024) 170827

Contents lists available at ScienceDirect

Science of the Total Environment

journal homepage: www.elsevier.com/locate/scitotenv

Imaging leachate runoff from a landfill using magnetotellurics: The Garraf karst case

A. Martí [a,*], P. Queralt [a], A. Marcuello [a], J. Ledo [b], G. Mitjanas [c], P. Piña-Varas [a], A. Freixes [d], J. Solà [d], P. Pons [d], J. López [d]

[a] Institut de Recerca Geomodels-UB, Facultat de Ciències de la Terra, Universitat de Barcelona, Spain
[b] Departamento de Física de la Tierra y Astrofísica, Facultad de Física, Universidad Complutense de Madrid, Spain
[c] Sustainable Minerals Institute, University of Queensland, Australia
[d] Geoservei Projectes i Gestio Ambiental S.L., Spain

HIGHLIGHTS

- A magnetotelluric study in a landfill has allowed imaging its electrical resistivity.
- Conductive zones are associated to the presence of leachate.
- Leachate penetrates through the landfill, thus affecting hydrological circulation.
- Magnetotellurics can tackle environmental studies that need great penetration depths.

GRAPHICAL ABSTRACT

A magnetotelluric (MT) study in a landfill (Garraf, Spain) allowed imaging the percolation of leachate below its base.

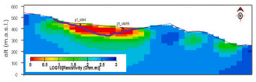

Vertical slice of the resistivity model. Highly conductive area (red) is attributed to leachate. The purple line marks the base of the landfill

This study shows the potential of MT in environmental studies when deep penetrations are required.

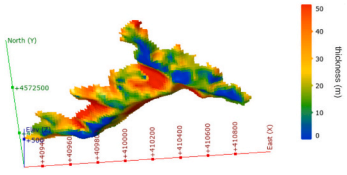

DEM of the landfill with values of the estimated thickness of leachate below the landfill base

ARTICLE INFO

Editor: Christian Herrera

Keywords:
Landfill
Leachates
Karstic drainage structure
Electrical resistivity
Magnetotellurics

ABSTRACT

Electrical and active source electromagnetic geophysical methods have been traditionally employed to approach and tackle environmental problems, such as those caused by landfills. However, since these problems are more consequential and cover broader areas, it is necessary to use deeper penetration methods, such as magnetotellurics. In the Garraf Massif (Catalan Coastal Ranges, NE Spain), an urban waste disposal landfill had been in operation from 1974 to 2006, during which >26 million metric tons of garbage had been deposited. This landfill overlies karstic terrain, thus principally impacting groundwater circulation. Previous electrical resistivity tomography profiles had partially imaged the infill but were not able to penetrate below the base of the original landfill. During 2019 and 2020 we performed a magnetotelluric study over the landfill and its surrounding with the goals of characterizing the electrical resistivity of the infill and below it. The 2D and 3D resistivity models confirmed the highly conductive nature of the leachate and allowed us to identify its presence below the landfill base, which we quantified with maximum thicknesses of 90 m. This proved that landfill leachate had filtered through the original impermeable layer, enhanced by the karstic drainage structure.

* Corresponding author.
E-mail address: annamarti@ub.edu (A. Martí).

https://doi.org/10.1016/j.scitotenv.2024.170827
Received 20 December 2023; Received in revised form 4 February 2024; Accepted 7 February 2024
Available online 12 February 2024

1. Introduction

Landfills are highly impactful environmental solutions to waste disposal, and should be the least preferable option, limited to the necessary minimum (EC, 2023). In Catalonia (NE Spain), despite the advances in garbage sorting and recycling, in 2021 34 % of urban waste still ended up in landfills (Agència Catalana de Residus (ACR), 2022). This evident reliance on landfills poses long-term environmental challenges because, even after their closure, their impact on the environment can last for many years, necessitating remediation and restoration actions.

The Garraf urban waste landfill is in the Vall de Joan valley, on top of the karstic Garraf Massif in the Catalan Coastal Ranges (Fig. 1), which has recently been designated as a natural protected space (Parc Natural del Garraf). The Garraf landfill was in operation between 1974 and 2006, with >26 million metric tons deposited (Entitat del Medi Ambient de l'Àrea Metropolitana de Barcelona (EMA), 2007). After its closure, decommissioning and restoration works were completed in 2021 (Àrea Metropolitana de Barcelona (AMB), 2021). A biogas plant, which mainly converts methane from the landfill into electricity, is still in operation.

Because of its karstic nature, the Garraf Massif constitutes an important underground hydrological system. Karst aquifers have well-known hydraulic and hydrogeologic characteristics that make them highly vulnerable to pollution from human activities (e.g., Hughes et al., 1994; De Waele et al., 2004, Simsek et al., 2011). The high permeability of these types of aquifers makes this geological setting one of the riskiest locations for landfills, the most characteristic issue being the short interval at which karst groundwater becomes polluted (Kačaroğlu, 1999). Therefore, although technical and scientific reports had warned against this project (e.g., Raventós and Senent, 1974), the landfill was constructed in order to respond to the high demand for urban waste from the metropolitan area of Barcelona. The base of the landfill was lined with presumed-to-be impermeable concrete to isolate the landfill from the geology below and to avoid the potential pollution of the underground waters (EMA, 2007). However, since the landfill was commissioned and continuing at present, there are reports of rainwater penetrating through the landfill, entraining leachate and other contaminants. In submarine outflows such as La Falconera (Garraf, Sitges, Fig. 1), or in cavities, anomalous values of contaminant gases have been recorded (Freixes et al., 2022).

It is well established that environmental impacts caused by urban waste landfills can be identified and quantified using geophysical methods. More particularly, electrical and active electromagnetic (EM) methods (e.g., Pous et al., 1996; Meju et al., 2000; Georgaki et al., 2008; Ramalho et al., 2012; Hajar et al., 2013; Casado et al., 2015) have allowed for characterization of the geometry of waste deposits and for the identification of leachate (including runoff) based on their low electrical resistivity. The magnetotelluric method (MT) (e.g., Chave and Jones, 2012) is a natural source electromagnetic method used to characterize the electrical resistivity of the subsoil. This can be associated to lithological composition and/or with the presence of fluids. There are few studies that use broadband MT to characterize landfills (audio-MT and radio-MT are more common for the typical depth range of landfills). The advantages of MT compared to active EM methods are its simpler field setup (MT does not require a transmitter), and its larger penetration depths, due to the broad range of frequencies of the natural EM fields. On the other hand, active EM methods have better resolution at shallow depths, and the measured signal is less affected by anthropogenic noise.

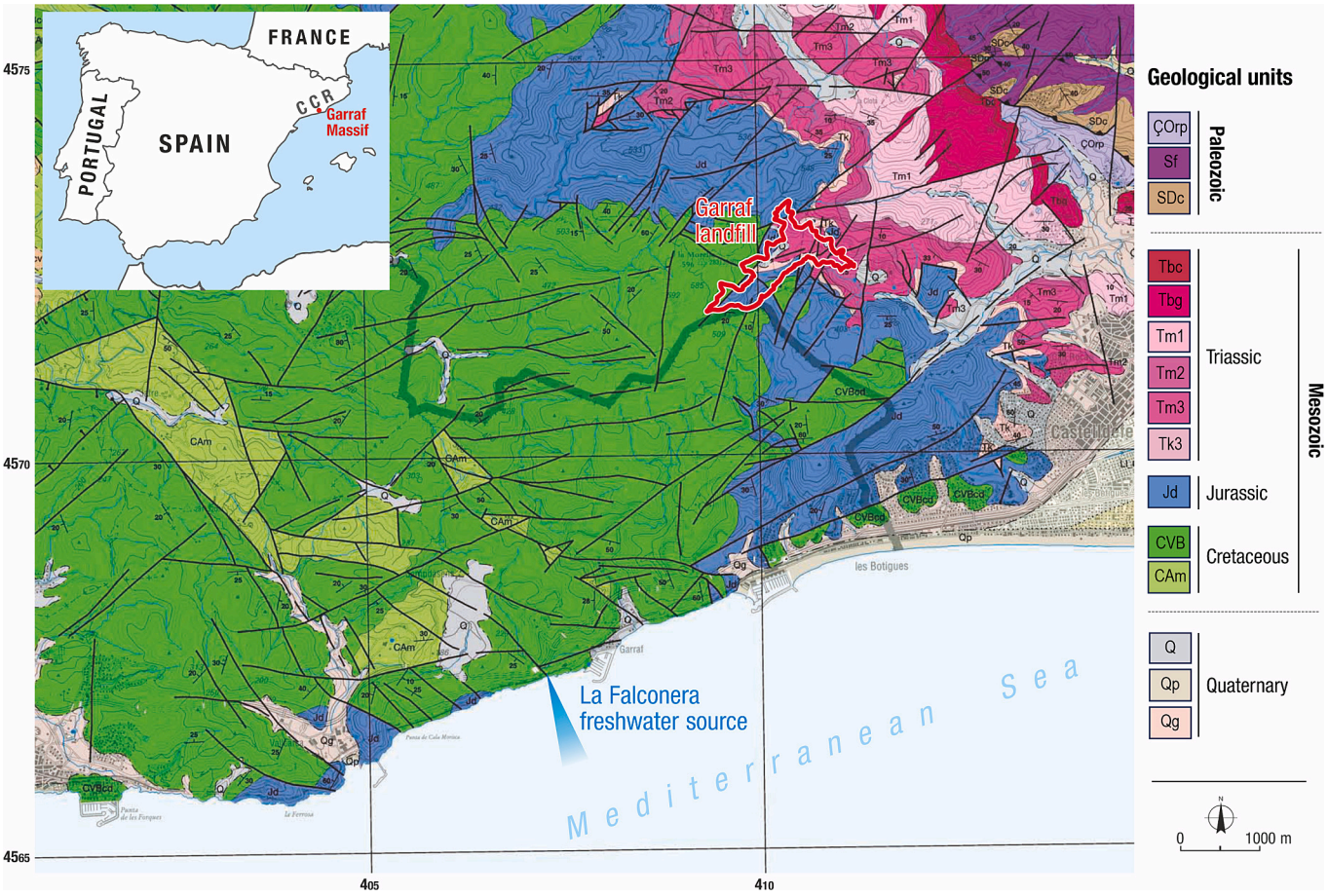

Fig. 1. Geological map of the study zone. Inset: Catalan Coastal Ranges (CCR). The red line indicates the perimeter of the Garraf landfill. Source: ICGC 1:50,000 map; modified by Geoservei.

Freixes et al. (2021) carried out an interdisciplinary study (hydrology, chemistry of organic pollutants, geochemistry and isotopes, microbiology and geophysics) to assess water quality in the Garraf Massif hydrogeological system, addressing the causes of bad odors in the La Falconera outflow. This study, which encompassed the municipalities surrounding the landfill, concluded that the landfill is the main source for the continuous and persistent influx of pollutants identified in the groundwater in the Garraf Massif.

The present work is focused on the geophysical aspect of the study, specifically via the use of the magnetotelluric method. Initially, several electrical resistivity tomography (ERT) profiles were acquired, which managed to image part of the infill in addition to the relevant pipes and man-made impermeabilization layers (concrete) (Cano et al., 2019). However, most of the profiles did not penetrate below the base of the landfill (to assess if the leachate had crossed it) nor to properly constrain its geometry. For this reason, we conducted a broadband magnetotelluric study to image the full volume of the landfill and to determine if the leachate had penetrated below the original base, and if so, to which extent.

2. Materials and methods

2.1. Geological setting

The Garraf landfill is located in the Vall de Joan valley (in the municipalities of Begues and Gavà) and the adjacent area, which belongs to the Garraf Massif, part of the Catalan Coastal Ranges (Fig. 1). The Garraf Massif forms a horst that delimits the tectonic graben of the Vallès-Penedès Basin to the North and the Mediterranean Sea to the South (Roca et al., 1999). The southern boundaries that define the coastline also respond to extension faults (e.g., Barcelona Fault). This extensional structure affects the massif and its limits and is part of the tectonic macrostructure that has been defined as the Valencia Trough in the Western Mediterranean (Roca and Guimerà, 1992; Roca, 1994).

The Garraf Massif is composed mainly of Paleozoic and Mesozoic rocks. Paleozoic units are predominantly formed by metapelitic and metapsamitic rocks, which constitute the basement and outcrop at the eastern end of the massif. Mesozoic materials are mostly carbonate rocks (limestone and dolomite), and properly define the massif that extends from the lower valley of the Llobregat (located in the east) to the valley of the river Foix (in the west). There are also minor appearances of conglomerates, sandstones, shales, and marls. Carbonate materials include the Triassic, Jurassic, and Cretaceous successions. The Triassic consists of the classical succession formed by the Buntsandstein (conglomerates, sandstones and shales), Muschelkalk (carbonates, sandstones and shales) and Keuper (carbonates, shales, gypsums and cellular dolomites). The materials that we are interested in highlighting for the purposes of this study are from the Jurassic to the Cretaceous, which occupy most of the massif's extension and specifically include limestones, dolomites, and marls (Fig. 1). The units that comprise the Garraf Massif are highly affected by different deformation events, Hercynian (affecting only Paleozoic rocks), Alpine, and post-Alpine (causing the generation and reactivation of folds and faults) (Guimera, 1982; Marin et al., 2023). The later Miocene extensional context has played the most recent role in developing the SW-tilted horst and graben structure that characterizes the present topography. Jurassic and Cretaceous rocks reach thicknesses of up to 1500 m in some parts of the massif (Freixes et al., 2021), and have developed an important karst system — a result of the complex structural evolution of the area (Cervelló and Freixes, 1992). In addition, more than six phases of karstification have been recognized from the Oligocene to the Pleistocene-Holocene.

From ca 23,000 years to the present, the subsurface hydrological system (with diffuse and karstic flow) has been affected by a 120 m rise in the sea level. This changed environment has disrupted the karst circulation, creating a saturated zone of general imbibition, and almost causing the extinction of the pre-existing karst circulation (Cervelló and Freixes, 1992). Despite the present low-pressure gradient and the diffuse type of flow, in episodes of significant recharge, there is a certain karst response. This can be observed in the La Falconera outflow (Fig. 1), which is sourced from the recharge areas of the Vall de Joan, where the Garraf landfill is located. Consequently, the strong recharges cause an important transfer of pollutants from the Garraf landfill to the sea (Freixes et al., 2021). Moreover, the pollutants are incorporated into the karstic drainage and constitute a tracer of underground water flow (Freixes, 2020).

This interdisciplinary study was carried out in the Jurassic and Cretaceous karst of the southern part of the massif, in order characterize the urban landfill's effect on the general karst environment of Vall de Joan, and its hydrogeological environment in particular.

2.2. The magnetotelluric method

The magnetotelluric method (MT) is a non-invasive electromagnetic technique that works in the frequency domain and allows us to obtain the resistivity distribution of the subsurface (Chave and Jones, 2012). The time variations of the horizontal electric (**E**) and magnetic (**H**) fields are measured at the surface, from which the frequency dependent transfer functions can be obtained. The impedance tensor (Z) is a 2 × 2 tensor with complex components:

$$\begin{bmatrix} E_x \\ E_y \end{bmatrix} = \begin{bmatrix} Z_{xx} & Z_{xy} \\ Z_{yx} & Z_{yy} \end{bmatrix} \begin{bmatrix} H_x \\ H_y \end{bmatrix}. \quad (1)$$

The components of Z can be converted into apparent resistivity (ρ_a), which is an average resistivity of the volume of Earth probed at a particular frequency (ω), and phase (φ), which provides additional information on the variations of the imaged structures:

$$\rho_{aij} = \frac{1}{\mu_0 \omega} |Z_{ij}(\omega)|^2, \quad (2)$$

$$\varphi_{ij}(\omega) = tan^{-1}\left[\frac{Im\ Z_{ij}(\omega)}{Re\ Z_{ij}(\omega)}\right], \quad (3)$$

where μ_0 is the magnetic permeability of free space and i and j refer to any of the horizontal components (x or y). These transfer functions can then be inverted to obtain a volume distribution of the electrical resistivities of the subsoil. In a karstic context, saturated cavities, fractures or fluid-filled conduits (salt or mineral water, or leachate) will produce a lower resistivity than the surrounding rock (limestone or dolomites) (Wang et al., 2017). Regarding the characterization of a landfill, the signature of leachate will show very low values of electrical resistivity. Laboratory studies of leachate solutions in distilled water give electrical resistivities on the order of 0.1 to 8 Ω·m depending on their concentration (Yoon et al., 2002). However, if the cavities are empty, the resistivity will be higher than the surrounding rock.

2.3. Data acquisition, processing and analysis

The MT survey was conducted over the landfill and its surroundings, consisting of a total of 100 sites (although 3 of them were located far from the landfill, and were not included in the study). Data were acquired in two stages, the first one in October 2019, and the second one between January and May 2020 (with a mandatory pause in April 2020 due to the Covid-19 pandemic).

The first stage was a proof-of-concept to obtain an initial estimate of the data quality, such as to evaluate the MT responses over a supposedly highly conductive area, and to assess the feasibility of a subsequent detailed study over the whole landfill. 10 MT sites were distributed along a roughly 800 m-long NW-SE profile that crosses the landfill and is partially coincident with an electrical tomography profile carried out by Cano et al. (2019) (Fig. 2). In the second stage, 87 MT sites installed: 83 within the landfill—with a roughly regular spacing between them—and 4 on its outskirts. Together with the profile dataset, it resulted in a high-density dataset of almost 100 sites, creating an adequate input data set for inversion to obtain a 3D high resolution resistivity model. Data were

acquired using METRONIX ADU-07e systems, non-polarizable electrodes, and magnetic coils MFS06 and MFS07. Electrical dipoles were between 15 and 25 m long, aligned along geographic NS and EW directions.

Time series were processed using Mapros software (Metronix, Friedrichs, 2003), based on a robust Fast Fourier Transform scheme to obtain the transfer functions (impedance tensor) in the frequency domain. It involved a visual inspection and selection of the time segments, digital filtering of LF (128 Hz to 32 Hz) and the use of different Parzen window widths. A digital filtering of the signal to 4 Hz was also applied with the purpose of reaching lower frequencies. In most cases, we observed that the apparent resistivities displayed an abrupt increase and that their phases dropped to 0°. This is an indication of correlated electrical signal (or noise) that overlaps the natural signal. Hence, the results of this band (4 Hz) were not considered in the further steps.

Fig. 3 shows the apparent resistivity and phases obtained for 6 representative sites (circled in yellow in Fig. 1). Sites 41 and 43 are located just outside the landfill (41 over Cretaceous materials, in the west, and 43 over Triassic rocks, in the east). Sites 13 and 30 are inside the landfill, over Jurassic rocks. Sites 53 and 80 are situated inside the landfill, over Triassic deposits. At a first glance, we see that, for sites outside the landfill, the apparent resistivity curves begin at short periods (high frequencies) with values on the order of 1000 Ω·m (site 41) and 100 Ω·m (site 43). In contrast, for sites located within the perimeter of the landfill (13, 30, 53, and 80), we notice the significantly lower values of the apparent resistivity (between 1 Ω·m and 10 Ω·m). These low values can be generalized to all the sites inside the landfill (see Fig. C3 in Appendix C) and can be attributable to the nature of the materials inside the landfill.

Due to the tensorial nature of impedance, the MT method is uniquely capable of allowing us to determine whether the geoelectric structure being characterized is 1D, 2D or 3D (for a given site and at a specific frequency). It therefore determines the variations of vertical and horizontal electrical resistivity. In addition, for the two-dimensional case, the main direction of the geoelectric structure (or strike) can be determined. This dimensionality can be determined from the analysis of the relationships of the tensor components, a method known as dimensionality analysis (e.g., Martí, 2006).

For the data acquired in the first stage, we performed a 2D hypothesis test (Strike code, McNeice and Jones, 2001) to assess its directionality (assuming 2D structure). We performed this for each site separately and for all the sites together, obtaining a direction of 27.6° (Fig. 4). The phase tensor (Caldwell et al., 2004) is another indication of the type of dimensionality. The results, shown in the appendix (Fig. A1 in Appendix A), are quite variable, with a central part at long periods indicating strike values of 20°–30°; the high values of the skew angle imply 3D effects. The phase tensor analyses indicate 3D geoelectrical structures, in agreement with the geometry of the study area. However, the 2D hypothesis test indicates a strike direction of about 28°. Given the layout of the sites and the results of this analysis, we proceeded to construct a 2D electrical resistivity model, using an inversion process, which is explained in the next section.

WALDIM1.1 code analysis (Martí et al., 2009) is based on the rotational invariants of the impedance tensor. The fact that these invariants are above or below a threshold value allows us to establish a criterion for determining whether the measured tensor corresponds to 1D, 2D, or 3D structures. In the case of 2D, it is also possible to determine the strike. For the second stage data, we used the WALDIM 1.1 code for

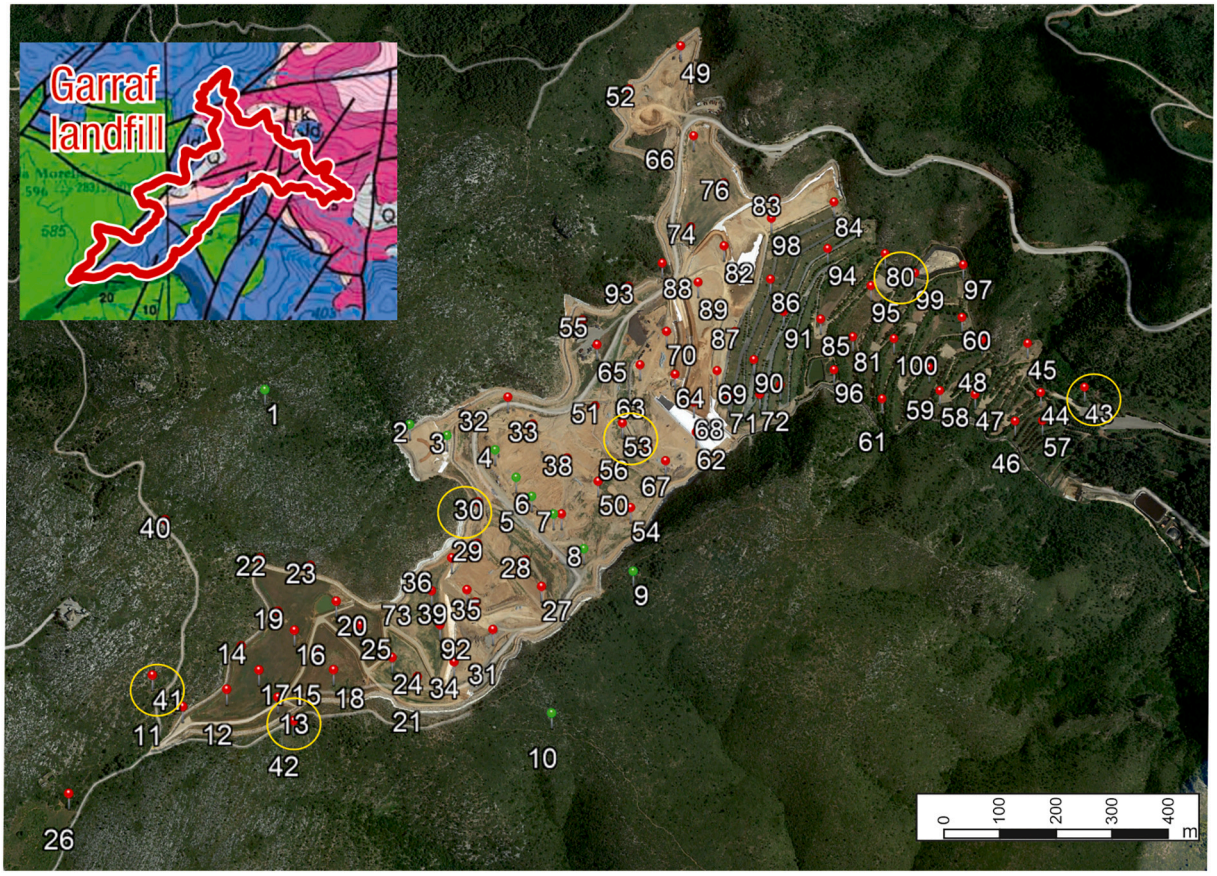

Fig. 2. Satellite image of the landfill (Google Earth, June 2020). This image shows how the eastern part of the landfill was already restored at the time of the study (covered with vegetation). MT site locations shown in red (green for profile 1 sites) acquired on top or in the nearest surroundings. The representative sites showing the apparent resistivity and phase curves in Fig. 3 are circled in yellow. Inset: detail of the geology of the landfill extracted from Fig. 1.

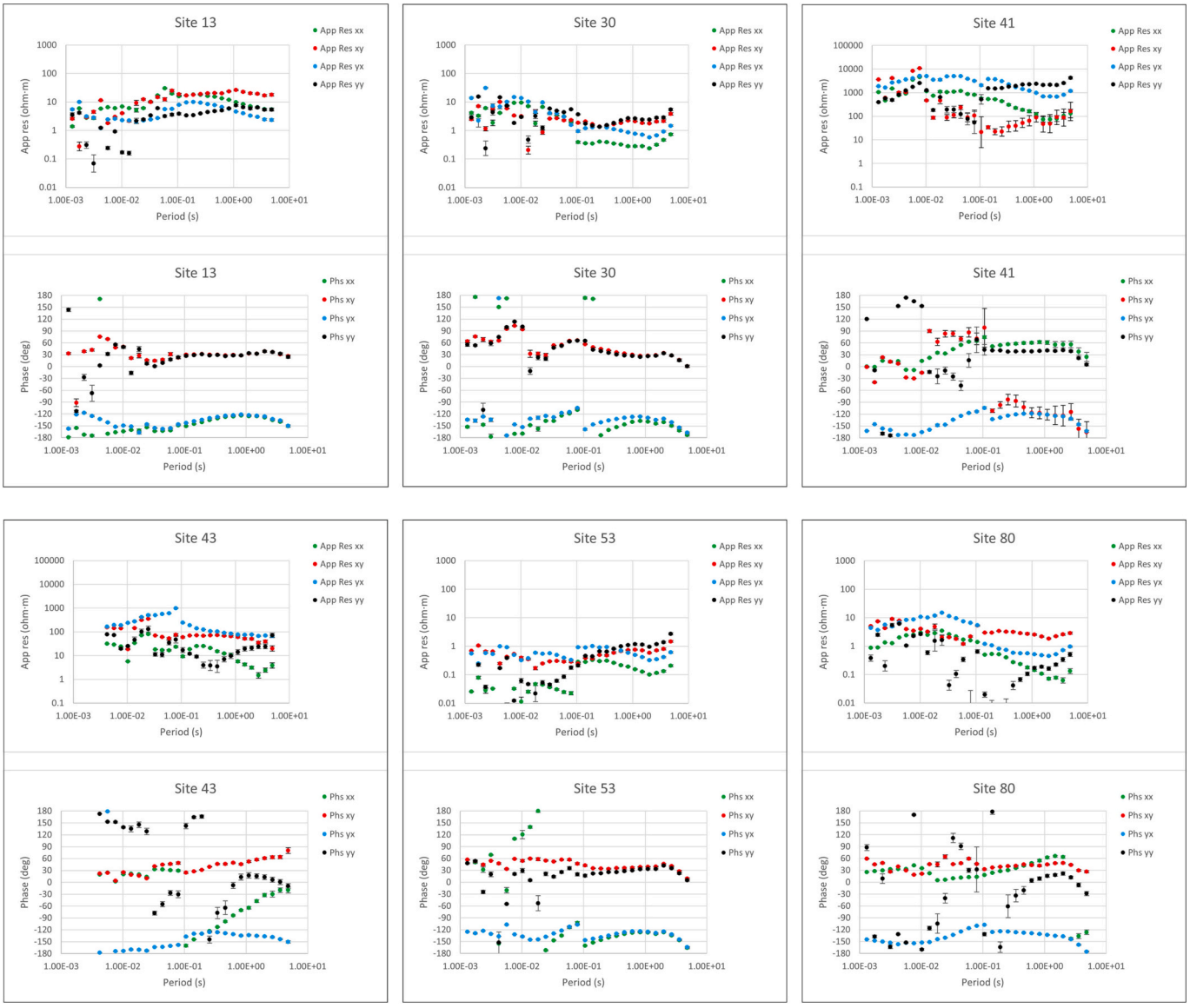

Fig. 3. Apparent resistivities and phases with their errors for 6 sites representative of the landfill and surroundings. Notice the different apparent resistivity scales for Sites 41 and 43 (outside the landfill) and Sites 13, 30, 53 and 80 (inside the landfill: more conductive values).

dimensionality analysis, with the expected outcomes being a general 3D geoelectrical structure (Fig. A2 in Appendix A).

2.4. 2D and 3D inversions

With the sites acquired in the first stage, and based on the obtained strike direction (28°), we considered a profile with a WNW-ESE orientation, below which the 2D model would be derived after data inversion. Site 8 was discarded because of out-of-quadrant phases (which can be attributed to 3D effects), and site 10 was discarded because it was too far from the profile location.

The 2D inversion, consisting of finding the 2D model that best fits the data, was performed using the Rodi and Mackie (2001) code implemented in Winglink® software. The 8 sites considered (1, 2, 3, 4, 5, 6, 7, and 9) were projected over the WNW-ESE (or 62°W, perpendicular to strike) profile. Data were rotated accordingly (28°E), and the resulting modes were assigned as TE (transversal electric, y′x′ in this case) and TM (transversal magnetic, x′y′). We applied a static shift correction and data outliers were manually deactivated. Finally, the resulting curves were smoothed using D+ (Beamish and Travassos, 1992) (see dots in Fig. B.1 in Appendix B) and we used periods between 10^{-3} and 3 s.

We then created a 2D mesh of 115 × 145 cells, considering the topography, and bathymetry towards the ESE end. In the upper and central part, the cell dimensions were 4 m × 4 m and increased in depth and towards the sides of the profile. The initial model consisted of a homogeneous resistivity of 50 Ω·m. For the seawater layer a value of 0.3 Ω·m was assigned and set as constant for the inversion. The type of inversion was a smooth inversion (which prioritizes the search for a smooth model with gradual resistivity contrasts) with a smoothing parameter of 3; and a standard Laplacian operator for the regularization. The difference between the model responses and the measured data is quantified through the rms (root mean square):

$$\mathrm{rms} = \frac{1}{Ndata}\sqrt{\sum_{i=1}^{\mathrm{Ndata}} \frac{(\mathrm{data_i} - \mathrm{response_i})^2}{(\mathrm{error\_data_i})^2}}, \tag{4}$$

With the full dataset (data acquired in both the first and second stages) the electrical resistivity of the landfill area was characterized using 3D inversion. For this work, we used the 3D ModEM inversion code (Kelbert et al., 2014). This made it possible to obtain a 3D model of

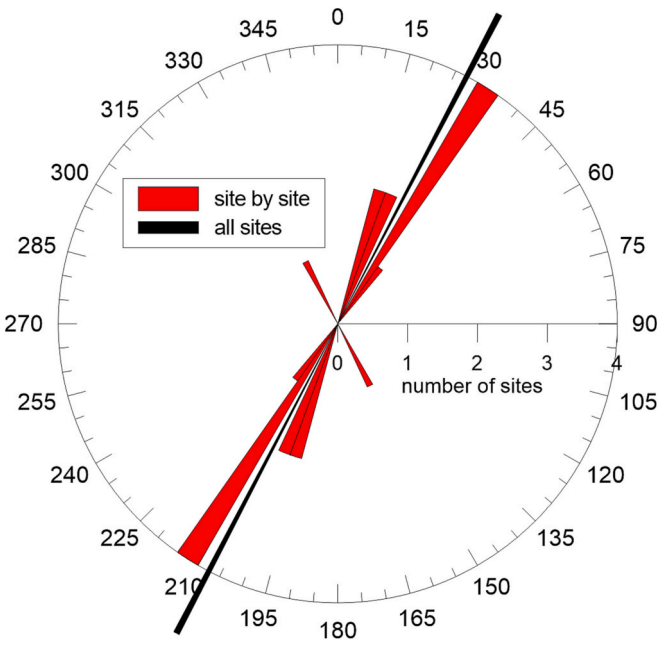

Fig. 4. Dimensionality analysis results for sites 1–10 corresponding to the first stage acquisition using strike analysis for the 2D hypothesis test.

the electrical resistivity of the landfill area, as well as its lateral and in-depth continuation. We first constructed a 3D model mesh oriented along the N(x), E(y), and vertical (positive downwards) (z) directions consisting of 81 × 96 × 55 cells that measured 23.6 km × 23.0 km × 36.0 km. In the central part of the model (where the MT sites were acquired), the horizontal size of the cells was 40 × 40 m^2. Vertically, the grid size was 20 m at the top, increasing with depth, as the shallower part must account for the topography and also because the MT data resolution decreases with depth. Specific values of the resistivity were given to the initial model (usually a homogeneous value), which included the air (resistivity value of 10^{10} Ω·m) and the sea (0.3 Ω·m). Initially, the 97 sites acquired inside the landfill and just outside its perimeter were considered but sites 8, 82, and 87 (because of their out-of-quadrant phases) and site 7 (very close to site 37) were discarded. Thus, 93 sites were ultimately used in the new inversions. The xy and yx components were inverted, with 5 % error assigned to the data.

3. Results

3.1. 2D model

The final 2D model, MT-2D, was obtained after several consecutive inversions of about 300 iterations each, refining the model successively. The initial rms, corresponding to the homogeneous 50 Ω·m model, was 32.23; and that of the final model was 3.07.

The apparent resistivity curves and phases of the measured data and model responses, and the individual rms for each site are shown in Appendix B (Fig. B1a and B1b). Site 1 is the one with the highest rms, while the others have values of around 3 or less.

We conducted sensitivity tests to assess the main structures imaged in the model and whether they were necessary to fit the data as they appear in the model, or if they could be modified (conductivity or geometry) or simply removed. All the details are explained in Appendix B. After these tests, we decided to remove a conductive body from the model, just ESE of site 9, which was not strictly necessary to fit the data. The resulting model is shown in Fig. 5, with the resistivity scale used in MT: red for the lowest resistivities (conductors) and blue and violet for the highest resistivities (by convention, the inverse color scheme to electrical tomography). In this case, the scale ranges from 0.1 Ω·m to 10,000 Ω·m. Fig. 5 also shows the pseudo-sections of apparent resistivity and phases of the TE and TM modes. The similarity between the pseudo-sections of the data and the model corroborates this good fit.

On its WNW side, the model presents an extensive resistive zone with values between 200 Ω·m and 10,000 Ω·m, extending from the surface to the bottom of the model. Towards the center, this resistive zone detaches from the surface level and dips towards the ESE. Within this resistive zone, there is a highly resistive zone (>10,000 Ω·m), located below sites 2 and 3, between 425 and 300 m a.s.l. Towards the ESE, a smaller resistive zone (2000 Ω·m) can be identified between sites 7 and 9, which dips towards the WNW and extends between the surface and 300 m a.s.l. At the ESE end of the model, below site 9, there is another large resistive zone (200 Ω·m near the surface and >10,000 Ω·m below 400 m a.s.l.); it also extends from the surface to the bottom of the model.

One of the most notable structures of the model is the highly conductive area (0.1 Ω·m–1 Ω·m) in the center of the model, between sites 2 and 7, that goes from the surface to a maximum depth of 400 m a.s.l. Within this zone, below site 4, an even more conductive zone (<0.1 Ω·m), reaching greater depths (350 m a.s.l.), stands out. An additional highly conductive area is located between sites 7 and 9 (>0.1 Ω·m). Between the most conductive part and the highly resistive zone at the ESE part of the model, a more extensive and moderately conductive zone (10 Ω·m) extends from the surface and continues towards sites 5, 6, and 7, below the main conductive area, reaching depths between 200 m a.s.l. and the sea level.

3.2. 3D model

We obtained the MT-3D model by departing from an initial 200 Ω·m model, while keeping the topography and bathymetry fixed. The initial rms was 368, and after 86 iterations it dropped to 5.2. Sites inside the landfill are those that show the lowest rms. All the model horizontal layers, vertical sections of the central part of the model and misfits between the measured data and calculated responses for each MT site are presented in Appendix C (Fig. C3).

Fig. 6 shows a selection of five horizontal layers of the central part of the model, with the position of the sites. For the top layers, the white part corresponds to air. In all the layers, one can observe high resistivity values outside the landfill area (100–1000 Ω·m), and highly conductive values inside the landfill perimeter (<10 Ω·m). The most conductive areas have values of <1 Ω·m (red colors in the figure), and are located between the surface and a maximum depth of 240 m a.s.l. The zone with the highest conductivity values (<1 Ω·m) displaces from the SW to the N and NE following the topography. Below this zone, the resistivity values are slightly higher and the horizontal extension of the conductor decreases.

Fig. 7 displays EW-oriented vertical sections, from north to south and from surface to sea level. Highly conductive areas (from red, <1 Ω·m to yellow, 5 Ω·m) can be identified extending from the surface and penetrating below the landfill vessel (indicated by the purple line corresponding to the topography of 1967, prior to landfill operations). As we move further down, the resistivity increases gradually, but not homogeneously. Although the minimum of the resistivity scale is 1 Ω·m, it should be noted that the resistivity values can be as low as 0.01 Ω·m, which is an exceptionally low value for this geological setting. Outside the landfill, we also observe that, in general, the resistivity values are higher in the W than in the E. Regarding the high resistivity zones surrounding the landfill, they have larger values and a greater extension in the W part than in the E part.

We extracted a cross section of the MT-3D model that was coincident with the location of the 2D model MT-2D (Fig. 8). The general resistivity distribution is maintained in its upper part. At larger depths, the 3D models lose resolution, which is an inherent effect of the inversion dimension (3D vs 2D). This effect may have also been amplified by the highly conductive values at the top of the model, which shield electromagnetic waves. However, we can still easily observe that both models

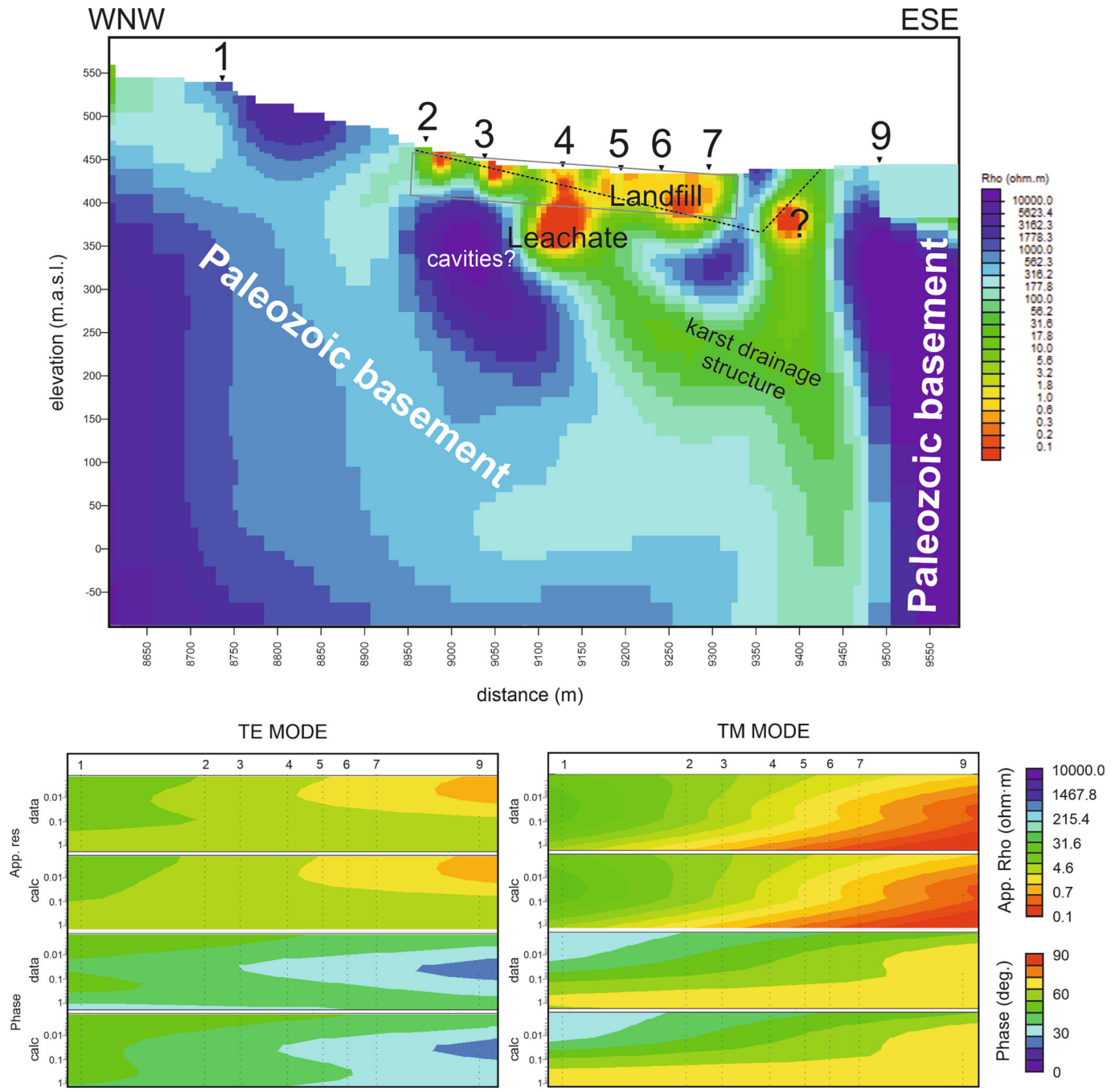

Fig. 5. Top: 2D electrical resistivity final model, MT-2D, with its interpretation. Discontinuous black line indicates the position of year 1967 topography (base of the landfill). The rectangular area surrounded by a grey line indicates the range of investigation of the previous ERT study. Bottom: Pseudo sections of the measured (data) and calculated (calc) apparent resistivities and phases, as a function of period, corresponding to the TE and TM modes.

show the conductive part inside the landfill, and how it continues below its base. Outside the landfill, both models are characterized by high resistivity values. Between sites 7 and 9, the section of the 3D model does not show the conductive zone (C7_9) that appeared in the 2D model. Instead, it shows a gradual increase in resistivity as we move from site 7 to site 9. In both cases, there are no sites in between, but the 3D model is more reliable because the inversion has also considered sites outside the profile. At the far end of the section, past site 9, the 3D model shows moderate resistivity values, which are not as high as in the 2D model (Fig. 5) but do agree with the sensitivity tests performed.

To assess the validity and resolution of the main structures of the model we performed four sensitivity tests, consisting of modifying the model, computing the responses of the modified model and comparing the rms obtained with the original one. In some cases, we let it run more iterations. Two of these tests concerned the shape and depth extent of the shallow conductor and allowed us to determine if it is necessary for the conductor to penetrate the base of the landfill (test 1), and if its bottom (located at about 100 m a.s.l) could be at shallower depths due to the loss in resolution (test 2). Hence, we kept its original geometry in the final model. Test 3 was made to assess if the model would present a change in resistivity between the Jurassic (karstified, highly resistive) and Triassic (less resistive) sediments. It proved that the model is compatible with this contrast located at 300 m a.s.l., as indicated by well measurements (PZ07, Vall del Teix, Anufra/Catalana de Perforacions,

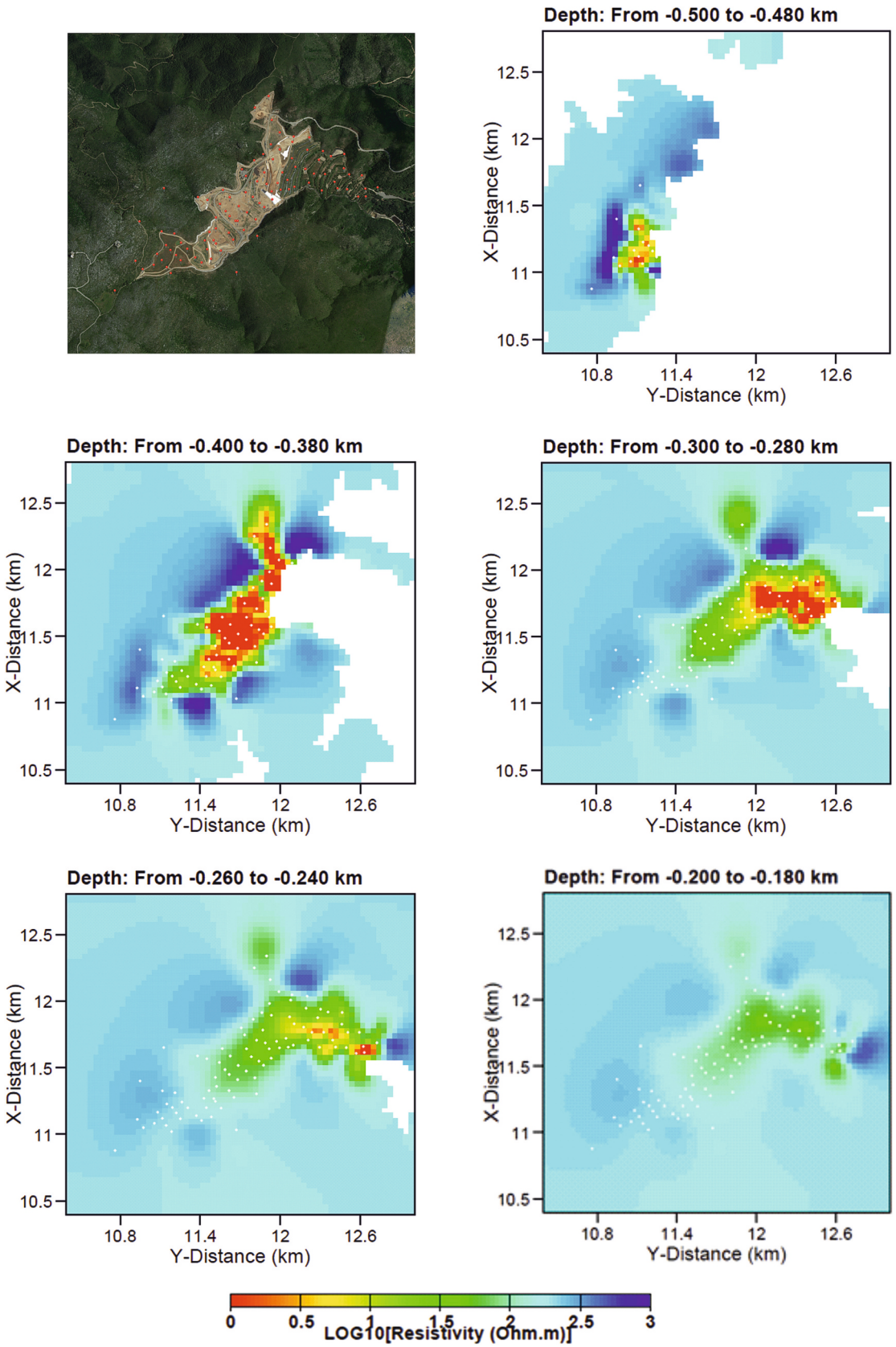

Fig. 6. Top left: satellite image of the landfill and surrounding area, corresponding to the central part of the 3D model, 3D-MT, and the location of the MT sites. Top right and rest of panels: selection of horizontal slices of the central part of the model, from the shallowest part to 180 m a.s.l. Note that by using ModEM notation the negative depths correspond to values above sea level.

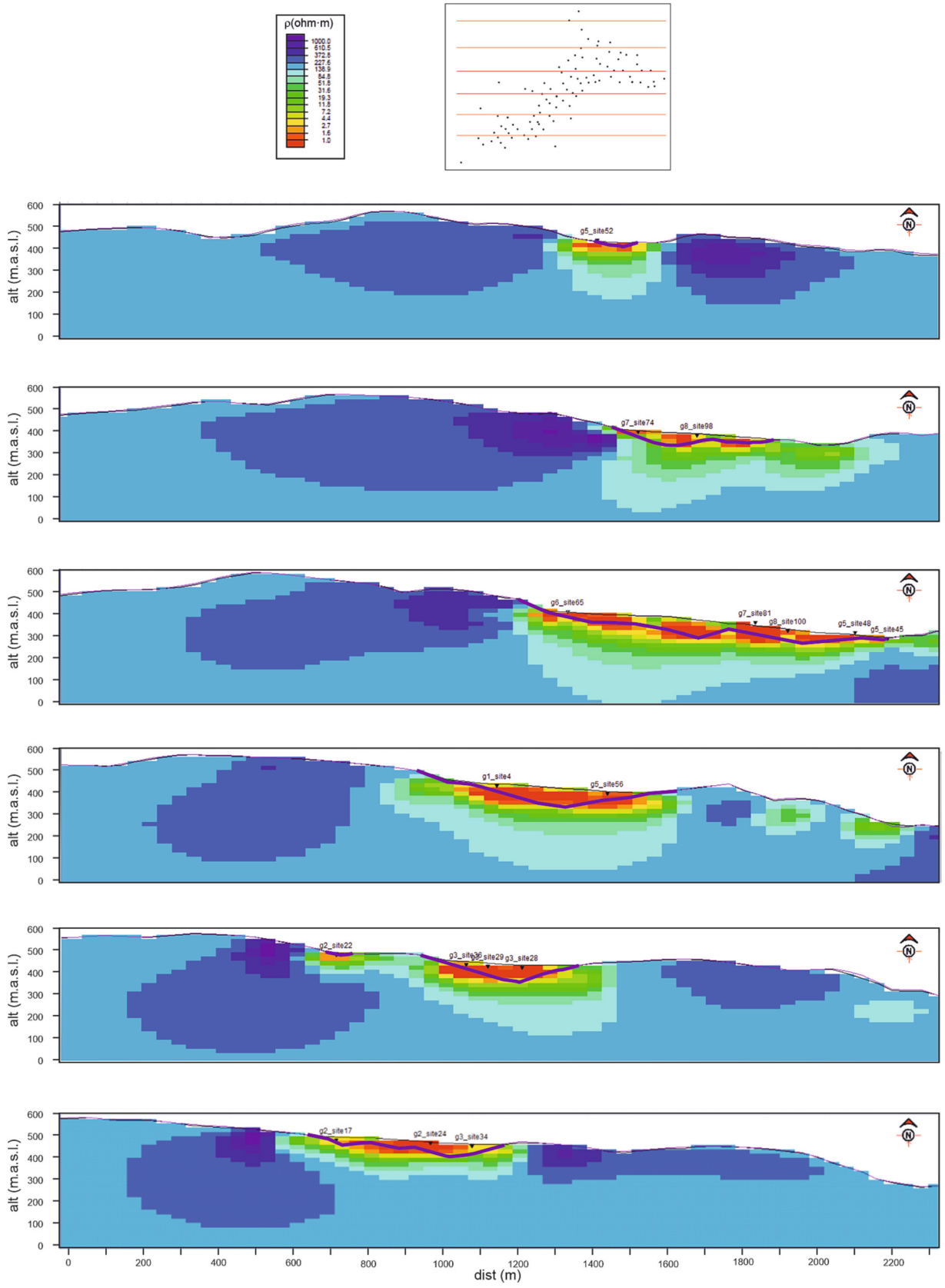

Fig. 7. Top: Plan view with the location of the sites and position of the vertical sections of the model (red lines) shown on the bottom panels. Bottom panels: Vertical sections of the upper central part of the MT-3D model, from north to south. Each section shows the current topography (black line, which corresponds to the upper limit of the model) and the topography of 1967 (purple line).

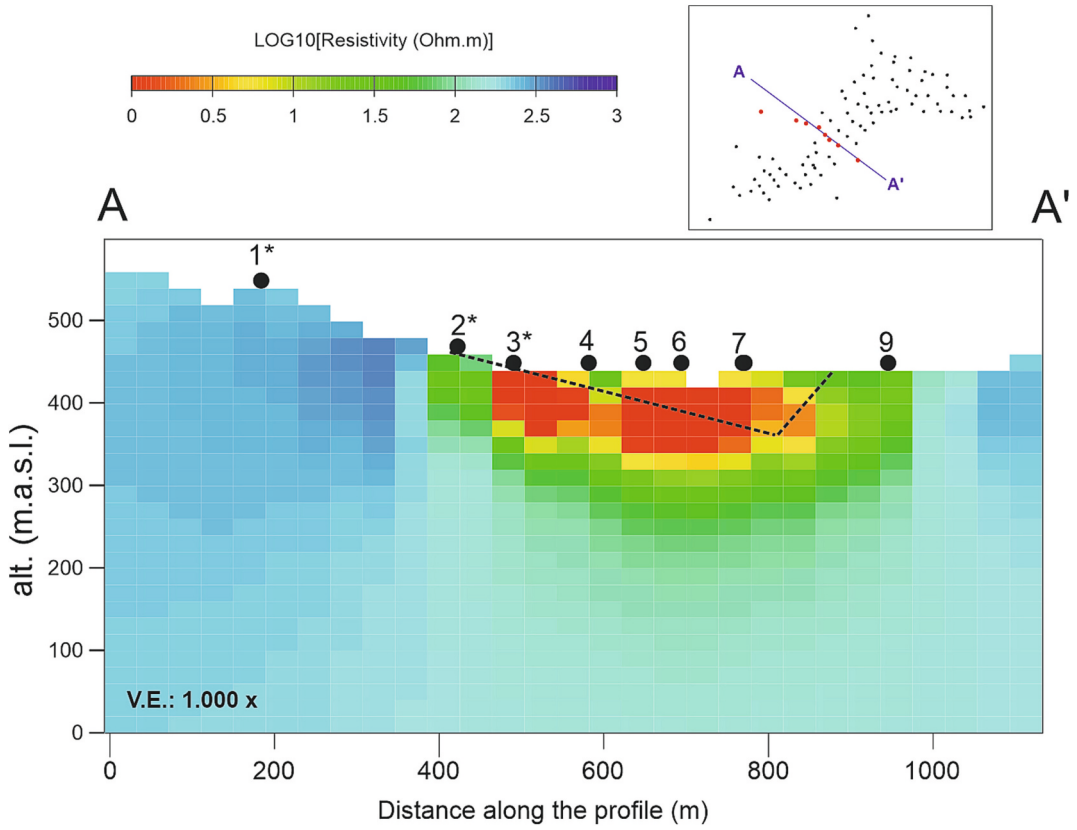

Fig. 8. Cross section of the model MT-3D along the profile used to obtain the 2D model, MT-2D. The discontinuous black line indicates the position of year 1967 topography (base of the landfill). Sites marked with a star (*) are located outside the cross section.

pers. Comm.). The results of these tests are explained in more detail in Appendix C (Figs. C4, C5, C6, and Table C1).

4. Discussion

From the geoelectrical features observed in the 2D and 3D models, we have interpreted them while considering geological and other geophysical information.

As already explained, the MT-2D model was co-located with the electrical tomography profile PTE-LONG. This profile is 720 m long, and the resulting model reached a depth of 360 m a.s.l. (Fig. 5). In the WNW, this model identified high values of resistivity (>2000 Ω·m) associated with the rocky bedrock and with the presence of the ostensibly impermeable concrete sheet that was previously installed to prevent leaching; the lower resistivity values are identified as a possible inflow of water or leachate. In the ESE, resistivity values on the order of 1 Ω·m to 5 Ω·m corresponded to the volume occupied by the landfill. Due to their nature, the two methods complement each other. While the tomography model gives a high-resolution image of the first 50 m below the surface, the MT model does not have as much resolution at the surface (for example, it cannot account for the concrete sheet) but allows for reaching greater depths below the base level of the landfill. The latter is an important point because with MT it has been possible to image not only the landfill infill, but also below it.

In Fig. 5 we have overlain the interpretation of the conductive and resistive structures from the 2D model. The shallowest part, between sites 2 and 9, located inside the landfill, is characterized by very high conductivities that cover the entire depth of the landfill. The high conductivity is attributed to the presence of leachate (e.g., Yoon et al., 2002). The fact that the high conductivity zone continues below the base of the landfill, especially below site 4, strongly suggests percolation of leachate beyond the landfill limits.

The highly resistive zones mark the rocky bedrock of the area surrounding the landfill (karst). The highest values of resistivities below sites 2 and 3 (over Cretaceous sediments), but not below site 4 (over Triassic), can be attributed not only to different geological units, but also to the presence of cavities, which increase electrical resistivity. The moderately conductive area below the ESE part of the landfill, despite not having a well-defined depth, could be associated with the fluid circulation of the karstic drainage structure.

The 3D model (Figs. 6, 7, and 8) has given us both a broader and a more precise interpretation of the study area. It represents the spatial distribution of conductivity within the landfill, which is clearly associated with the presence of leachate. Despite the loss of resolution at the bottom of the conductor, the fact that the conductivity values decrease with depth can be attributed to a decrease in the leachate concentration as it percolates through the surrounding rocks. Moreover, it confirms that the conductive values continue below the landfill, indicating that the leachate has traversed its base layer. We have quantified how much of this leachate is below the landfill by plotting the thickness of the values that have a resistivity value of <5 Ω·m, below the landfill base (Fig. 9 top). These values vary between 0 and 90 m (Fig. 9 bottom left). The zone where the leachate penetrated the least is located in the NE sector of the landfill. Its thickness is largest just to the west. As we move towards the SW, the thickness decreases along the central part of the landfill and increases towards its sides. For illustration, we plotted a contour map of these thicknesses overlain on the geological map, showing Cretaceous, Jurassic, and Triassic units, cut by numerous faults (Fig. 9 bottom right). The fact that the thickness of the leachate is higher in this area might be due to the presence of faults. In Appendix D, we included a video (Garraf.mp4) that shows different views of the 3D model within its local and geological context. It specifically presents a vertical section that shows the electrical resistivity distribution and the limits of the landfill.

In the surroundings of the landfill, resistive zones correspond to the rocky substrate, in accordance with the 2D model. They present higher resistivity values corresponding to areas of higher karstification—predominantly in the west—where the rocks are of Cretaceous age and happen to be more karstified.

This model is in agreement with the hydrogeological information (Freixes et al., 2021), which indicates that the transfer of leachate occurs through the karst drainage structure that goes from the Vall de Joan to La Falconera: first, the circulation occurs in the unsaturated zone (rapid infiltration and underground runoff) followed by a rapid transition to the saturated zone that partly discharges due to the outflow of La Falconera where it meets the sea, but also offshore.

5. Conclusions

We have conducted a magnetotelluric survey in a landfill located in the Garraf Massif. The geoelectrical resistivity models obtained through 2D and 3D inversion, and validated through sensitivity tests, have provided us with the characterization of the landfill's infill and the underlying basement rocks, and the extent of leachate penetration.

The surroundings of the landfill are characterized by high resistivity values, attributed to highly karstified Cretaceous and Jurassic units with

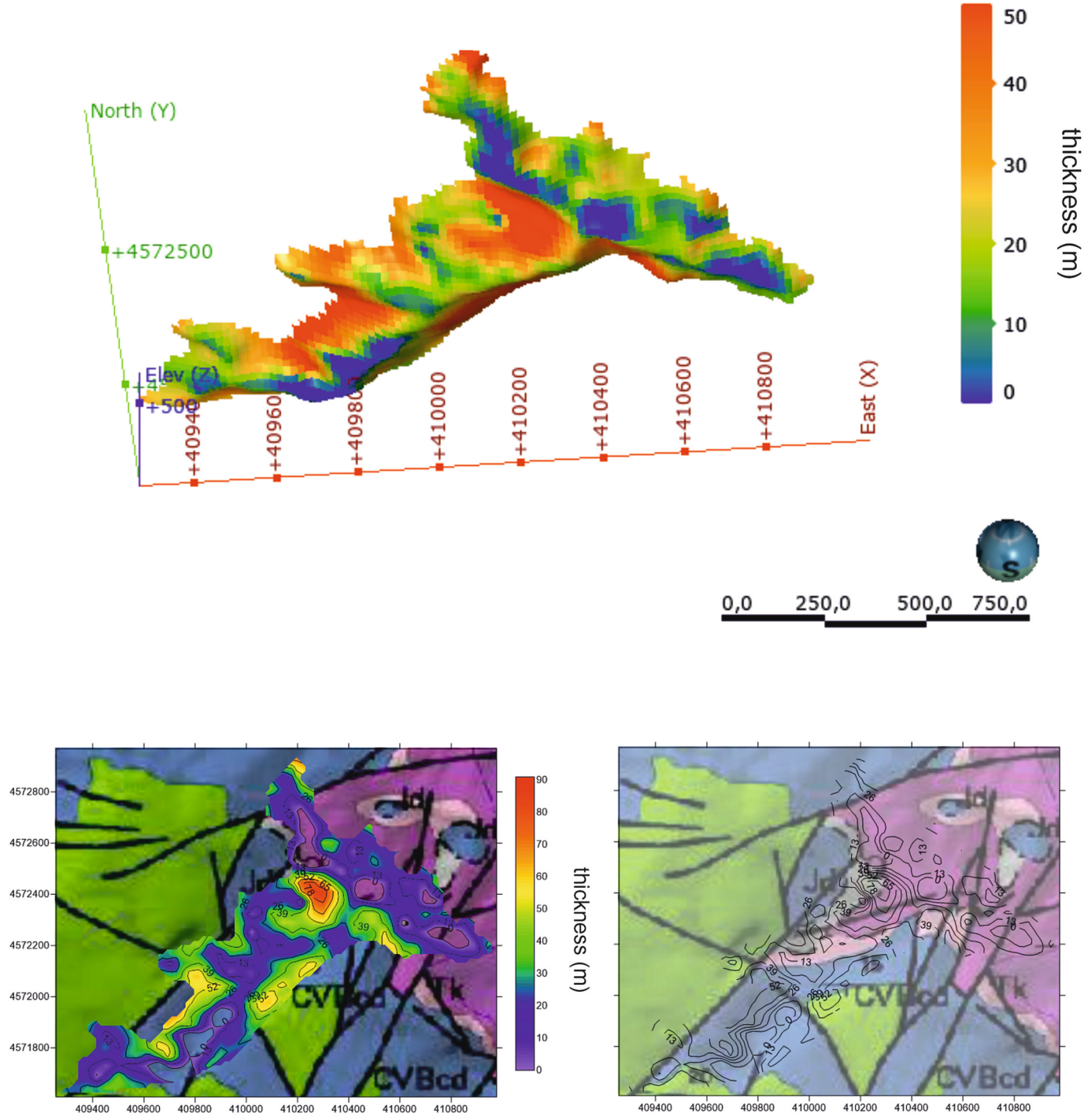

Fig. 9. Top: 3D representation of the landfill base topography with the thickness of the conductive body below it. Coordinates in UTM (m) Bottom: higher resolution representation of the contours of the thickness of the conductive body over the geological map (ICGC, 2016). This figure was generated using © Seequent software.

hollow cavities. Less conductive zones can be attributed to fluid circulation in faults.

Inside the landfill, a highly conductive volume extends from the surface to the base of the landfill and continues below its original topography, which is interpreted as due to the presence of leachate that penetrates below the landfill (between 0 and 90 m depth). The model aligns with hydrogeological findings, suggesting leachate transfer through a karst drainage structure from Vall de Joan to the La Falconera outflow.

In addition to characterizing the electrical structures of the Garraf landfill and its surroundings, for the first time we are able to identify and delineate the presence of leachate that penetrated beneath the original permeabilization of the landfill using geophysical techniques. The inclusion of topography in the resistivity models makes the MT method suitable to be applied in landfills with different geometric settings (valley-type, slope or above/under-ground landfills). This study highlights the potential of the MT method compared to active electrical and EM methods as it can reach deeper targets, making it suitable to resolve current and future environmental problems that need characterization at depth.

CRediT authorship contribution statement

A. Martí: Writing – review & editing, Writing – original draft, Methodology, Investigation, Formal analysis, Data curation, Conceptualization. **P. Queralt:** Writing – review & editing, Methodology, Investigation, Formal analysis, Data curation, Conceptualization. **A. Marcuello:** Writing – review & editing, Methodology, Investigation, Formal analysis, Data curation, Conceptualization. **J. Ledo:** Writing – review & editing, Methodology, Investigation, Formal analysis, Data curation, Conceptualization. **G. Mitjanas:** Writing – review & editing, Methodology, Investigation, Formal analysis, Data curation, Conceptualization. **P. Piña-Varas:** Writing – review & editing, Methodology, Investigation, Formal analysis, Data curation, Conceptualization. **A. Freixes:** Writing – review & editing, Investigation. **J. Solà:** Writing – review & editing, Investigation. **P. Pons:** Writing – review & editing, Investigation. **J. López:** Writing – review & editing, Investigation.

Declaration of competing interest

The authors declare that they have no known competing financial interests or personal relationships that could have appeared to influence the work reported in this paper.

Data availability

Data will be made available on request.

Acknowledgements

We thank Gary Egbert and co-authors for providing the ModEm code and Naser Meqbel for allowing the use of the 3D Grid software. We acknowledge the Àrea Metropolitana de Barcelona (AMB) and the company Tirssa for having allowed us to carry out this study. We gratefully thank the editor Christian Herrera and an anonymous reviewer for their helpful comments.

Appendix A. Supplementary data

Supplementary data to this article can be found online at https://doi.org/10.1016/j.scitotenv.2024.170827.

References

Agència Catalana de Residus (ACR), 2022. Principals magnituds 2021 de la gestió de residus municipals [Press Dossier]. http://estadistiques.arc.cat/ARC/estadistiques/Residus%20municipals%202021_Principals%20magnituts_Dossier.pdf.

Àrea Metropolitana de Barcelona (AMB), 2021. Conclou l'operació de clausura i segellament de l'antic abocador del Garraf i s'accelera la seva integració al parc natural [Press release]. https://www.amb.cat/es/web/amb/actualitat/sala-de-premsa/notes-de-premsa/detall/-/notapremsa/conclou-l-operacio-de-clausura-i-segellament-de-l-antic-abocador-del-garraf/11970181/11696.

Beamish, D., Travassos, J.M., 1992. The use of the D+ solution in magnetotelluric interpretation. J. Appl. Geophys. 29, 1–19.

Caldwell, T.G., Bibby, H.M., Brown, C., 2004. The magnetotelluric phase tensor. Geophys. J. Int. 158, 457–469.

Cano, A., Juanola, R., Claveria, J., 2019. Prospecció geofísica mitjançant tomografia elèctrica al dipòsit de residus del Garraf, Barcelona (Fase II). Technical Report. GS Ingenieria.

Casado, I., Himi, M., Lovera, R., Fernández, J., Casas, A., 2015. Use of electrical tomography methods to determinate the extension and main migration routes of uncontrolled landfill leachates in fractured areas. Sci. Total Environ. 506–507, 546–553. https://doi.org/10.1016/j.scitotenv.2014.11.068.

Cervelló, J.M., Freixes, A., 1992. El domini càrstic. In: Història Natural dels Països Catalans 2. Geologia II (Geomorfologia). Enciclopèdia Catalana, Barcelona, pp. 461–508.

Chave, A.D., Jones, A.G. (Eds.), 2012. The Magnetotelluric Method: Theory and Practice. Cambridge University Press. ISBN: 9780521819275.

De Waele, J., Nyambe, I.A., Di Gregorio, A., Di Gregorio, F., Simasiku, S., Follesa, R., Nkemba, S., 2004. Urban waste landfill planning and karstic groundwater resources in developing countries: the example of Lusaka (Zambia). J. African Earth Sci. 39 (3–5), 501–508. https://doi.org/10.1016/j.jafrearsci.2004.07.014.

Entitat del Medi Ambient de l''Àrea Metropolitana de Barcelona (EMA), 2007. El dipòsit controlat de la Vall de Joan. Tres dècades de gestió dels residus municipals a l'Àrea Metropolitana de Barcelona, pp. 1974–2006. ISBN: 9788487881022.

European Commission (EC), 2023. Waste Framework Directive. European Commission. https://environment.ec.europa.eu/topics/waste-and-recycling/waste-framework-directive_en (Last access 15/12/2023).

Freixes, A., 2020. Els aqüífers càrstics dels Pirineus de Catalunya. Interès estratègic i sostenibilitat. Tesi doctoral (2014). Facultat de Geologia. Universitat de Barcelona. Reedició de la tesi doctoral. Kras, Hidrologia experimental.

Freixes, A., Solà, J., Pons, P., López, J., Bayés, C., Casas, A., Cervelló, J.M., Aceves, M., Otero, N., Soler, A., Carrey, R., Caixach, J., Bartolomé, A., Ballesté, E., García-Aljaro, C., Lucena, F., Blanch, A.R., Martí, A., Queralt, P., Marcuello, À., Ledo, J., 2021. La qualitat de l'aigua del sistema hidrogeològic del Garraf i les seves implicacions. Estudi per analitzar les causes d'olors a la surgència de la Falconera encaminat a minimitzar el seu impacte al poble del Garraf. In: Informe Final. Geoservei, S.L. AMB.

Freixes, A., Pons, P., Solà, J., 2022. Informe sobre el control del sistema hidrogeològic del Garraf. Control de gasos a les cavitats de la zona no saturada del carst. Període Abril–Desembre de 2021a. In: Geoservei, S.L. AMB.

Friedrichs, B., 2003. MAPROS, Magnetotelluric Processing Software (Metronix). User Manual.

Georgaki, I., Soupios, P., Sakkas, N., Ververidis, F., Trantas, E., Vallianatos, F., Manios, T., 2008. Evaluating the use of electrical resistivity imaging technique for improving CH_4 and CO_2 emission rate estimations in landfills. Sci. Total Environ. 389, 522–531.

Guimera, J., 1982. Estudi estructural de les zones de fractura de Garraf i de Vallcarca (Massís de Garraf). Institut d'Estudis Catalans, 1982–96 pp.

Hajar, B., Piga, C., Loddo, F., Ranieri, G., Messari, J., Ouazani Touhami, A., 2013. Geophysical surveys for the characterization of landfills. Int. J. Innov. Appl. Stud. 4 (2), 254–263 (ISSN: 2028-9324. ZDB-ID: 2703985).

Hughes, T.H., Memon, B.A., Lamoreaux, P.E., 1994. Landfills in karst terrains. Environ. Eng. Geosci. xxxi (2), 203–208. https://doi.org/10.2113/gseegeosci.xxxi.2.203.

ICGC, 2016. Mapa geologic comarcal 1:50.000, MGC50m v2. www.icc.cat/vissir3/.

Kačaroğlu, F., 1999. Review of groundwater pollution and protection in karst areas. Water Air Soil Pollut. 113, 337–356. https://doi.org/10.1023/A:1005014532330.

Kelbert, A., Meqbel, N., Egbert, G., Tandon, K., 2014. ModEM: a modular system for inversion of electromagnetic geophysical data. Comput. Geosci. 66, 40–53. https://doi.org/10.1016/j.cageo.2014.01.010.

Marín, M., Roca, E., Baqués, V., Cantarero, I., Cabrera, L., Ferrer, O., Travé, A., 2023. Fluid-rock interaction control on fault reactivation: a review of the Montmell-Vallès Fault System, central Catalan Coastal Ranges (NE Iberia). Global Planet. Change 220, 104011. https://doi.org/10.1016/j.gloplacha.2022.104011.

Martí, A., 2006. A Magnetotelluric Investigation of Geoelectric Dimensionality and Study of the Central Betic Crustal Structure. PhD Dissertation,. Universitat de Barcelona, 306 pp. http://www.tdx.cat/TDX-0115107-115853S.

Martí, A., Queralt, P., Ledo, J., 2009. WALDIM: a code for the dimensionality analysis of magnetotelluric data using the rotational invariants of the magnetotelluric tensor. Comput. Geosci. 35, 2295–2303.

McNeice, G., Jones, A.G., 2001. Multisite, multifrequency tensor decomposition of magnetotelluric data. Geophysics 66, 158–173.

Meju, et al., 2000. Geoelectrical investigation of oldrabandoned, covered landfill sites in urban areas: model development with a genetic diagnosis approach. J. Appl. Geophys. 44, 115–150.

Pous, J., Queralt, P., Chavez, R., 1996. Lateral and topographic effects in geoelectric soundings. J. Appl. Geophys. 35, 237–248.

Ramalho, E., Dill, A.M.M., Rocha, R., 2012. Assessment of the leachate movement in a sealed landfill using geophysical methods. Environ. Earth Sci. 68 https://doi.org/10.1007/s12665-012-1742-8.

Raventós, J.A., Senent, J., 1974. Informe sobre el proyectado vertedero controlado de basuras de Garraf. Escuela Catalana de Espeleología. In: Catálogo Espeleológico del Macizo de Garraf (II). Unidad meridional del macizo. J. Borràs. Barcelona.

Roca, E., 1994. La evolucion geodinamica de la Cuenca Catalano-Balear y areas adyacentes desde el Mesozoico hasta la actualidad. Acta Geol. Hisp. 29, 3–25.

Roca, E., Guimera, J., 1992. The Neogene structure of the eastern Iberian margin: structural constraints on crustal evolution of the Valencia Trough (western Mediterranean). Tectonophysics 203, 203–218.

Roca, E., Sans, M., Cabrera, L., Marzo, M., 1999. Oligocene to Middle Miocene evolution of the central Catalan margin (northwestern Mediterranean). Tectonophysics 315, 209–233.

Rodi, W., Mackie, R.L., 2001. Nonlinear conjugate gradients algorithm for 2-D magnetotelluric inversion. Geophysics 66, 174–187.

Simsek, C., Yavuz, A.B., Elci, H., et al., 2011. Waste disposal on karstic terrain: a case study from the ancient marble quarries in Iznik (Nicaea), Turkey. Geosci. J. 15, 339–348. https://doi.org/10.1007/s12303-011-0021-0.

Wang, X., He, L., Chen, L., Xu, L., Li, J., Lei, X., Wei, D., 2017. Mapping deeply buried karst cavities using controlledsource audio magnetotellurics: a case history of a tunnel investigation in southwest China. Geophysics 82 (1), EN1–EN11. https://doi.org/10.1190/GEO2015-0534.1.

Yoon, G., Oh, M., Park, J., 2002. Laboratory study of landfill leachate effect on resistivity in unsaturated soil using cone penetrometer. Environ. Geol. 43, 18–28. https://doi.org/10.1007/s00254-002-0649.